Sixth International Symposium on Turbulence and Shear Flow Phenomena
Seoul, Korea, 22-24 June 2009

TOWARDS THE DEVELOPMENT OF RANS MODELS FOR CONJUGATE HEAT TRANSFER

Tim J. Craft, Hector Iacovides, Sakchai Uapipatanakul
Turbulence Mechanics Group
School of Mechanical, Aerospace & Civil Engineering,
The University of Manchester,
Manchester M60 1QD, UK
sakchai.uapipatanakul@postgrad.manchester.ac.uk

ABSTRACT

The present study is concerned with exploring the ability of eddy-viscosity based RANS models to compute conjugate heat transfer problems, including capturing the decay of turbulent temperature fluctuations across the wall region. This is done by extending the application of the modelled transport equations for temperature variance and its dissipation rate across the solid wall region, thus providing the decay of the variance across this region.

Comparisons are drawn with existing DNS data of plane channel flow, at a relatively low Reynolds number, heated through a wall of non-zero thickness. Cases are simulated covering a range of thermal activity ratios, representing a range of different solid/fluid thermal conductivity/diffusivity ratios. It is found that, in order to predict the correct decay of temperature variance across the wall, an accurate representation of it, and of its dissipation rate, in the near-wall fluid flow region is required. This, in turn, also requires an accurate representation of the near-wall dynamic field turbulence.

A number of modifications are proposed to an existing four-equation k-ε-$\overline{\theta^2}$-ε_θ model in order to provide good near-wall predictions of the four variables under the two limiting thermal boundary treatments of isothermal and isoflux conditions. The resulting scheme is shown to perform well in the conjugate calculations over a range of thermal activity ratios.

INTRODUCTION

Conjugate heat transfer is a crucial issue in a number of engineering fluid flow applications, including nuclear engineering and other power-generation and heat-exchanger equipment. In these situations it is often not sufficient to simply consider heat transport in the fluid, with some idealised boundary condition at the fluid/wall interface. Instead, one may need to consider the fully coupled problem, including heat conduction in the solid wall.

If the near-wall flow is turbulent, then the situation can become rather complex, since temperature fluctuations in the near-wall fluid lead to similar fluctuations in the temperature of the solid wall. These, in turn, can cause thermal stresses in the material, which may lead to fatigue and finally damage. It is thus desirable to be able to simulate such phenomena reliably, in order to avoid potential problems, and this clearly requires an accurate prediction method for both the dynamic and thermal field turbulence in the fluid, and also for the resulting penetration of the thermal fluctuations into the solid.

From an industrial point of view, it is also desirable to have relatively cheap computational methods, so the present study is performed within the Reynolds Average Navier Stokes (RANS) modelling framework. Eddy-viscosity based schemes have been employed to date, within a general four-equation modelling strategy to account for the dynamic and thermal field turbulence in the fluid region. The transport equations for the mean temperature, temperature variance, $\overline{\theta^2}$, and its dissipation rate, ε_θ, have been simultaneously solved across the solid region also, with suitable matching conditions for the thermal field at the fluid/solid interface, to provide the thermal field predictions across the solid.

From the analysis of Polyakov (1974), it is known that one relevant parameter in conjugate heat transfer problems is the thermal activity ratio (defined below, but essentially representing a measure of the relative thermal conductivities and diffusivities in the fluid and solid). The present work has thus focused on reproducing the results of the DNS study of Tiselj et al. (2001a), who simulated conjugate heat transfer in a plane channel flow for a range of thermal activity ratios, providing profiles of the resulting temperature variance across both the fluid and the solid channel wall.

Initial calculations have employed the four-equation scheme of Hanjalić et al. (1996). This was developed primarily for studying buoyancy-affected flows, in which the temperature variance influences the turbulent heat fluxes via buoyancy-related generation terms. The present case does not involve buoyancy effects, so all buoyancy-related terms have been omitted from the model. As will be shown, the scheme does not capture the penetration of the thermal fluctuations into the wall well, mainly as a result of predicting rather too low dissipation rates for turbulent kinetic energy and temperature variance in the immediate near-wall fluid region. In the work described below, therefore, a number of modifications to the model will be detailed, aimed at improving the near-wall predictions of both the turbulent dynamic and thermal fields. Particular attention is given to ensuring accurate thermal field predictions under the two idealised fluid thermal boundary conditions of a prescribed temperature or prescribed heat flux at the wall. It will be shown that these refinements generally also lead to improvements in the conjugate heat transfer predictions, over a range of thermal actvity ratios.

CASE STUDIED

The case studied here is that of flow through a plane channel of half-width H with a wall of non-zero thickness d uniformly heated at its outer edge (Figure 1). The relevant non-dimensional parameters for this problem are the flow Reynolds number, the non-dimensional wall thickness

$d^{++} = (u_\tau d/\nu)(\alpha_f/\alpha_w)^{0.5}$, where u_τ is the friction velocity and α_f, α_w the molecular thermal diffusivity of fluid and solid respectively, and the 'thermal activity ratio', K, defined as $K = (\lambda_f/\lambda_w)(\alpha_w/\alpha_f)^{0.5}$ where λ_f and λ_w are the molecular thermal conductivity of the fluid and solid. Of particular note is that the two limiting cases of $K = 0$ and $K = \infty$ correspond respectively to the two idealised situations typically considered in fluid-only studies, namely those of applying a fixed temperature (isothermal) or a fixed heat flux (isoflux) condition at the fluid/wall boundary.

DNS data for this case have been reported by Tiselj et al. (2001a) at a Reynolds number, based on friction velocity and channel half-width, of $Re_\tau = 150$, and Prandtl number 7, with $d^{++} = 20$ and a range of values of K. As noted above, some of the modelling effort reported here has been aimed at ensuring accurate near-wall predictions in the two limiting cases of isothermal and isoflux conditions. For this, further comparisons are also drawn with the DNS of Tiselj et al. (2001b) who reported non-conjugate heat transfer results at almost the same Reynolds number, but with a Prandtl number of unity, presenting temperature variance budgets for both isothermal and isoflux boundary condition cases.

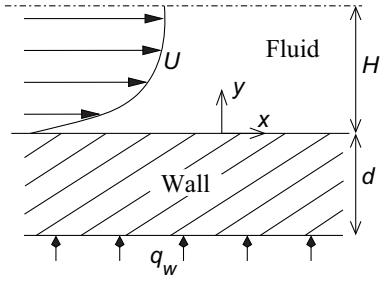

Figure 1: Geometry of problem considered.

TURBULENCE MODELLING

The initial calculations have employed the k-ε-$\overline{\theta^2}$-ε_θ scheme of Hanjalić et al. (1996) across the fluid region. In this, the Reynolds stresses are obtained from the Launder & Sharma (1974) (LS) k-ε model:

$$\overline{u_i u_j} = (2/3)k\delta_{ij} - \nu_t\left(\frac{\partial U_i}{\partial x_j} + \frac{\partial U_j}{\partial x_i}\right) \tag{1}$$

with $\nu_t = c_\mu f_\mu k^2/\tilde{\varepsilon}$, and k and $\tilde{\varepsilon}$ obtained from the transport equations

$$\frac{Dk}{Dt} = P_k - \varepsilon + \frac{\partial}{\partial x_j}\left[(\nu+\nu_t)\frac{\partial k}{\partial x_j}\right] \tag{2}$$

$$\frac{D\tilde{\varepsilon}}{Dt} = c_{\varepsilon 1}\frac{\tilde{\varepsilon}P_k}{k} - c_{\varepsilon 2}f_\varepsilon\frac{\tilde{\varepsilon}^2}{k} + \frac{\partial}{\partial x_j}\left[(\nu+\nu_t/\sigma_\varepsilon)\frac{\partial\tilde{\varepsilon}}{\partial x_j}\right] + E \tag{3}$$

where the generation rate $P_k = -\overline{u_i u_j}\,\partial U_i/\partial x_j$, the dissipation rate $\varepsilon = \tilde{\varepsilon} + \nu(\partial k^{1/2}/\partial x_j)^2$, and E is a modelled near-wall source term:

$$E = 2\nu\nu_t\left(\frac{\partial^2 U_i}{\partial x_j \partial x_k}\right)^2 \tag{4}$$

The various model coefficients and damping terms are given in Table 1, with the turbulent Reynolds number defined as $R_t = k^2/(\tilde{\varepsilon}\nu)$.

Table 1: Launder & Sharma (1974) k-ε coefficients.

c_μ	$c_{\varepsilon 1}$	$c_{\varepsilon 2}$	σ_ε
0.09	1.44	1.92	1.3

f_ε	f_μ
$1 - 0.3\exp(-R_t^2)$	$\exp(-3.4/(1+R_t/50)^2)$

Table 2: Hanjalić et al. (1996) $\overline{\theta^2}$ and $\tilde{\varepsilon}_\theta$ coefficients.

$c_{\varepsilon_\theta 1}$	$c_{\varepsilon_\theta 2}$	$c_{\varepsilon_\theta 3}$	$c_{\varepsilon_\theta 4}$	σ_t	$\sigma_{\varepsilon_\theta}$	c_{Et}
0.72	0.8	1.3	2.2	0.9	1.3	2.0

For the thermal field, transport equations are solved for the scalar variance, $\overline{\theta^2}$, and the homogeneous part of its dissipation rate, $\tilde{\varepsilon}_\theta$:

$$\frac{D(\rho c_p\overline{\theta^2})}{Dt} = 2\rho c_p P_\theta - 2\rho c_p\varepsilon_\theta + \frac{\partial}{\partial x_j}\left[c_p\left[\frac{\mu}{Pr}+\frac{\mu_t}{\sigma_t}\right]\frac{\partial\overline{\theta^2}}{\partial x_j}\right] \tag{5}$$

$$\begin{aligned}\frac{D(\rho c_p\tilde{\varepsilon}_\theta)}{Dt} &= c_{\varepsilon_\theta 1}\rho c_p\frac{P_k\tilde{\varepsilon}_\theta}{k} + c_{\varepsilon_\theta 3}\rho c_p\frac{P_\theta\tilde{\varepsilon}_\theta}{\overline{\theta^2}} \\ &\quad - c_{\varepsilon_\theta 4}\rho c_p\frac{\tilde{\varepsilon}_\theta^2}{\overline{\theta^2}} - c_{\varepsilon_\theta 2}\rho c_p f_{\varepsilon_\theta}\frac{\tilde{\varepsilon}\tilde{\varepsilon}_\theta}{k} + \rho c_p E_\theta \\ &\quad + \frac{\partial}{\partial x_j}\left[c_p(\mu/Pr + \mu_t/(\sigma_t\sigma_{\varepsilon_\theta}))\frac{\partial\tilde{\varepsilon}_\theta}{\partial x_j}\right]\end{aligned} \tag{6}$$

where c_p is the specific heat capacity, $P_\theta = -\overline{u_i\theta}\,\partial T/\partial x_i$, $\varepsilon_\theta = \tilde{\varepsilon}_\theta + \alpha(\partial\overline{\theta^2}^{1/2}/\partial x_j)^2$ and the modelled near-wall source term E_θ is given by

$$E_\theta = c_{Et}\alpha\alpha_t\left(\frac{\partial^2 T}{\partial x_i \partial x_j}\right)^2 \tag{7}$$

where $\alpha = \nu/Pr$ and $\alpha_t = \nu_t/\sigma_t$. Other model coefficients are given in Table 2.

Although Hanjalić et al. used a more elaborate algebraic formulation, to account for buoyancy effects, in this study the turbulent heat fluxes are modelled using a simple eddy-diffusivity formulation:

$$\overline{u_i\theta} = -(\nu_t/\sigma_t)\frac{\partial T}{\partial x_i} \tag{8}$$

with σ_t taken as 0.9.

The above formulation does mean that in this non-buoyant flow $\overline{\theta^2}$ and ε_θ do not influence the turbulent heat fluxes (and hence the mean temperature). However, they are still solved for, in order to provide the scalar variance variation across both fluid and solid regions.

The dynamic field equations are, of course, only solved across the fluid region, with boundary conditions $U = k = \tilde{\varepsilon} = 0$ at the wall. The mean temperature, $\overline{\theta^2}$ and $\tilde{\varepsilon}_\theta$ equations are solved across both solid and fluid regions, with a constant wall heat flux applied at the outer wall edge and suitable matching conditions at the fluid-solid interface. In the solid region the $\overline{\theta^2}$ and $\tilde{\varepsilon}_\theta$ equations take the simplified form

$$\frac{\partial(\rho c_p\overline{\theta^2})}{\partial t} = -2\rho c_p\varepsilon_\theta + \frac{\partial}{\partial x_j}\left[c_p(\mu/Pr)\frac{\partial\overline{\theta^2}}{\partial x_j}\right] \tag{9}$$

$$\frac{\partial(\rho c_p\tilde{\varepsilon}_\theta)}{\partial t} = -c_{\varepsilon_\theta 4}\rho c_p\frac{\tilde{\varepsilon}_\theta\tilde{\varepsilon}_\theta}{\overline{\theta^2}} + \frac{\partial}{\partial x_j}\left[c_p\frac{\mu}{Pr}\frac{\partial\tilde{\varepsilon}_\theta}{\partial x_j}\right] \tag{10}$$

which can be seen to be equivalent to equations (5) and (6). However, these are now, of course, applied using the density and specific heat capacity of the solid wall.

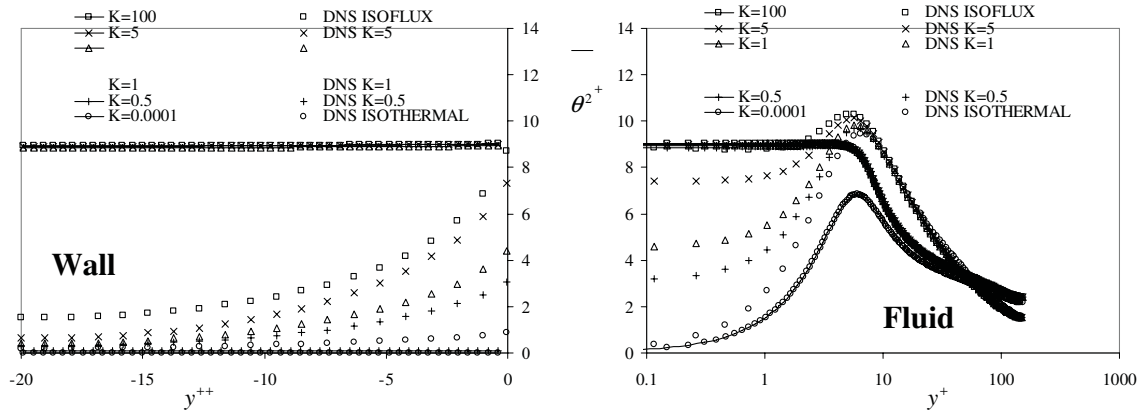

Figure 2: $\overline{\theta^2}$ profiles across the fluid and solid regions for different thermal activity ratios using the Hanjalić et al. (1996) scheme.

NUMERICAL TREATMENT

Since the flow is fully-developed, the governing transport equations have been solved using a 1-D finite volume based numerical solver, with 160 grid nodes across the fluid region and 50 across the solid, to ensure grid-independence of the results. Calculations have been performed for a range of thermal activity ratios, K, as well as for idealised isothermal and isoflux boundary condition cases. The latter two were achieved using the same solver, but setting K to 0.0001 and 100 respectively, which were found to well approximate the limiting cases of $K = 0$ and ∞ noted above.

INITIAL RESULTS

Previous results for this problem using the above model have been reported by Keshmiri (2006), and were reproduced in this study. Figure 2, for example, shows the resulting profiles of $\overline{\theta^2}$ across the fluid and solid regions for a range of thermal activity ratios, K. As can be seen, the DNS data show the level of temperature variance at the solid/fluid interface depends on K, and subsequently decays across the wall. The model does not reproduce the differences in the temperature variance across the fluid well over the range of thermal activity ratios tested, returning almost identical profiles for anything other than the isothermal case (ie. for any $K \neq 0$). It also gives an almost negligible decay of $\overline{\theta^2}$ across the solid wall.

The above weaknesses were traced, at least partly, to the near-wall modelling of the dynamic field and, in particular, the severe under-prediction of the near-wall dissipation rate ε when using the LS model (as shown in Figure 3). This, in turn, led to low values of the temperature variance dissipation rate ε_θ in the near-wall fluid region, and subsequently across the wall.

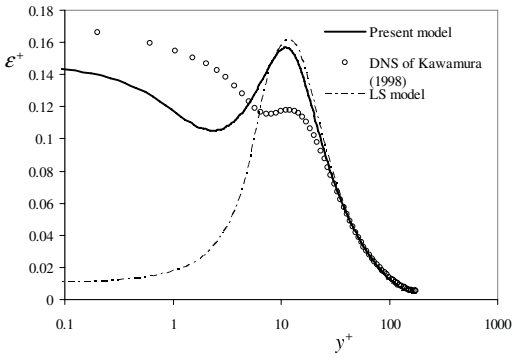

Figure 3: Near-wall ε profiles predicted by the Launder & Sharma (1974) and present models.

MODEL REFINEMENTS

To improve predictions of the dynamic field, some modelling elements based on those adopted in the three-equation non-linear eddy-viscosity model of Suga (1995), which is known to produce a significantly better near-wall variation of ε than the LS model, were incorporated into the present scheme.

One of the modifications adopted was to introduce a factor f_g into the modelling of turbulent diffusion in the k and $\tilde{\varepsilon}$ equations, giving

$$d_k = \frac{\partial}{\partial x_j}\left[(\nu + f_g \nu_t)\frac{\partial k}{\partial x_j}\right] \tag{11}$$

$$d_{\tilde{\varepsilon}} = \frac{\partial}{\partial x_j}\left[(\nu + f_g \nu_t/\sigma_\varepsilon)\frac{\partial \tilde{\varepsilon}}{\partial x_j}\right] \tag{12}$$

where $f_g = 5(\varepsilon/\tilde{\varepsilon})^{3/4} - 4$. The effect of this is to increase the level of turbulent diffusion close to the wall. A second modification was the introduction of a near-wall sink term in the $\tilde{\varepsilon}$ equation of the form

$$S_\varepsilon = -(\varepsilon - \tilde{\varepsilon})(\tilde{\varepsilon}/k)\exp(-R_t^2/100) \tag{13}$$

which acts to balance the molecular diffusion of $\tilde{\varepsilon}$ immediately adjacent to the wall. The third modification was the replacement of the near-wall source term E by the more elaborate form

$$E = c_{E1}\tilde{S}\nu_t\frac{k^2}{\varepsilon}\left(\frac{\partial^2 U_i}{\partial x_j \partial x_k}\right)^2 + c_{E2}\nu\frac{\nu_t}{k}\frac{\partial k}{\partial x_j}\frac{\partial U_k}{\partial x_l}\frac{\partial^2 U_k}{\partial x_j \partial x_l} \tag{14}$$

with coefficients tuned as $c_{E1} = 0.0022$ and $c_{E2} = -0.7$.

The resulting near-wall ε profile, also shown in Figure 3, is clearly a significant improvement on that of the original model. Moreover, as shown in Figure 4, the scheme still predicts a mean velocity profile in good agreement with the DNS data of Kawamura et al. (1998) at $Re_\tau = 180$, and correctly captures the logarithmic mean velocity profile over a wide range of channel flow Reynolds numbers.

When the above thermal field transport equations are solved in conjunction with this improved dynamic field representation, Figure 5 shows that in the limiting case of a constant wall temperature there is good agreement between the predicted mean temperature distribution, DNS data of Tiselj et al. (2001a) and the empirical log-law of Jayatilleke (1969) over a range of Prandtl numbers. Predicted Nusselt numbers were also found to agree well with empirical correlations over a wide range of Reynolds and Prandtl numbers.

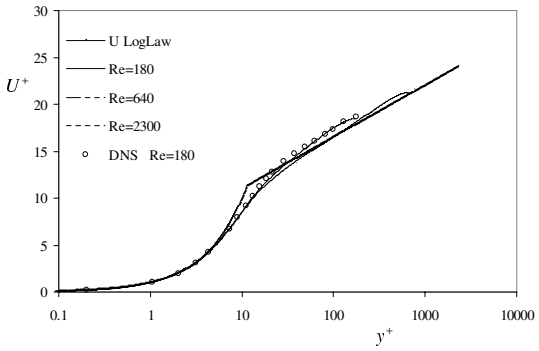

Figure 4: Predicted mean velocity profiles with the present model over a range of Reynolds numbers.

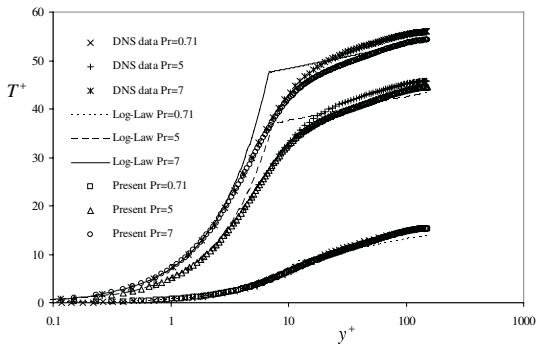

Figure 5: Mean temperature profiles for a range of Prandtl numbers.

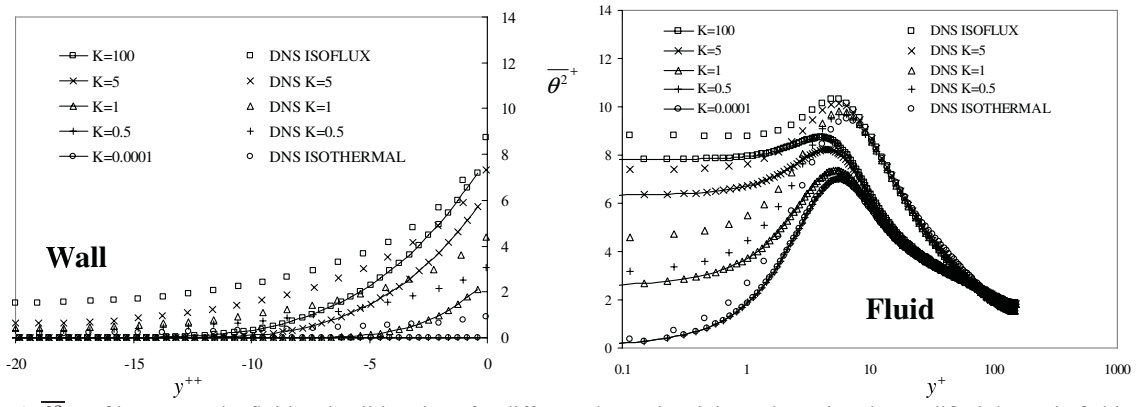

Figure 6: $\overline{\theta^2}$ profiles across the fluid and solid regions for different thermal activity ratios using the modified dynamic field model.

The conjugate heat transfer calculation results in Figure 6 show that the above modifications lead to significant improvements in the $\overline{\theta^2}$ profiles across both the fluid and solid regions. The results show an improved sensitivity to the thermal activity ratio, K, although at low (but non-zero) values of K the near-wall $\overline{\theta^2}$ tends to be particularly underpredicted (with the $K = 0.5$ case giving essentially identical results to the isothermal one), and the rate of decay of $\overline{\theta^2}$ across the solid is now rather too rapid.

To explore what further refinements might be included in the thermal field modelling, Figure 7 shows the predicted near-wall profiles of $\overline{\theta^2}$ and ε_θ for the two limiting cases of isothermal and isoflux boundary conditions, compared to the DNS of Tiselj et al. (2001 b). As can be seen, although $\overline{\theta^2}$ is not too badly predicted (albeit rather underpredicted in the isoflux case), the near-wall levels of ε_θ are significantly underpredicted for the isothermal case and overpredicted in the isoflux case. In an attempt to improve these predictions, similar modifications to those described above for the dynamic field modelling have been incorporated into the modelled $\overline{\theta^2}$ and $\tilde{\varepsilon}_\theta$ equations. In particular, the near-wall turbulent diffusion has been enhanced via the addition of the function f_g, as detailed above, giving

$$d_\theta = \frac{\partial}{\partial x_j}\left[c_p(\mu/Pr + f_g\mu_t/\sigma_t)\frac{\partial\overline{\theta^2}}{\partial x_j}\right] \qquad (15)$$

$$d_{\varepsilon_\theta} = \frac{\partial}{\partial x_j}\left[c_p(\mu/Pr + f_g\mu_t/(\sigma_t\sigma_{\varepsilon_\theta})\frac{\partial\tilde{\varepsilon}_\theta}{\partial x_j}\right] \qquad (16)$$

and a near-wall sink term has been included in the $\tilde{\varepsilon}_\theta$ equation of the form

$$S_{\varepsilon_\theta} = -c_{n1}(\varepsilon_\theta - \tilde{\varepsilon}_\theta)\frac{\tilde{\varepsilon}}{k}\exp(-R_t^2/10) \qquad (17)$$

with coefficient tuned as $c_{n1} = 0.8$.

Use of a more elaborate E_θ source term, analogous to that of equation (14) in the $\tilde{\varepsilon}$ equation, was also explored, but did not produce significant improvements. Hence, the original formulation for E_θ was retained, but with re-tuned coefficient $C_{Et} = 1.5$.

The resulting near-wall $\overline{\theta^2}$ and ε_θ profiles in the isothermal and isoflux cases are shown in Figure 8. As can be seen, the near-wall ε_θ is improved in the isothermal case, leading also to an improvement in the predicted $\overline{\theta^2}$ profile. However, although there is some improvement in the predicted $\overline{\theta^2}$ profile for the isoflux case, the near-wall ε_θ values in this case are still overpredicted.

The corresponding $\overline{\theta^2}$ profiles in the conjugate problem with intermediate thermal activity ratios are shown in Figure 9. As can be seen, there are significant further improvements in the profiles across the fluid, with distinct lines now visible for each value of K (and the sensitivity of $\overline{\theta^2}$ levels to K generally reproduced). Across the solid, however, although the distinct lines at different values of K are now visible, the predicted decay of $\overline{\theta^2}$ with distance is still rather too rapid.

A number of explorations have been carried out to identify what can be done to improve further the prediction of the near-wall ε_θ for the isoflux case. Whilst in the isothermal case the near-wall budgets of $\overline{\theta^2}$ and ϵ_θ are rather similar to those of k and ε, in the isoflux case θ does not go to zero at the wall (although $\partial\theta/\partial y$ does), leading to a more subtle balance of near-wall terms in the modelled $\tilde{\varepsilon}_\theta$ equation.

After some investigation, the only modification that appeared to significantly reduce the near-wall level of ε_θ in the isoflux case was to reduce the magnitude of the molecular diffusion term. Whilst this may, at first sight, not appear to be a particularly defensible modification, it should be recalled that molecular diffusion does not appear as an isolated term in the exact ε_θ equation. Instead, the molecular-related terms that

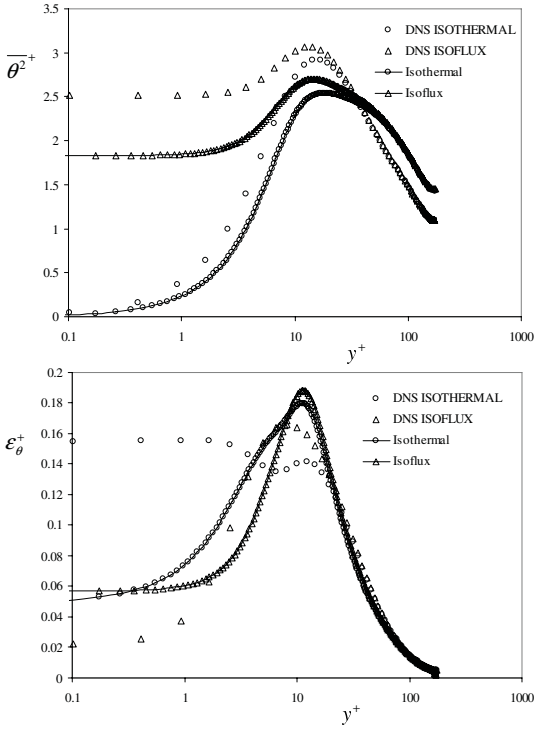

Figure 7: Near-wall $\overline{\theta^2}$ and ε_θ profiles for the limiting isothermal and isoflux thermal boundary condition cases using the Hanjalić et al. (1996) $\overline{\theta^2}$, $\tilde{\varepsilon}_\theta$ equations.

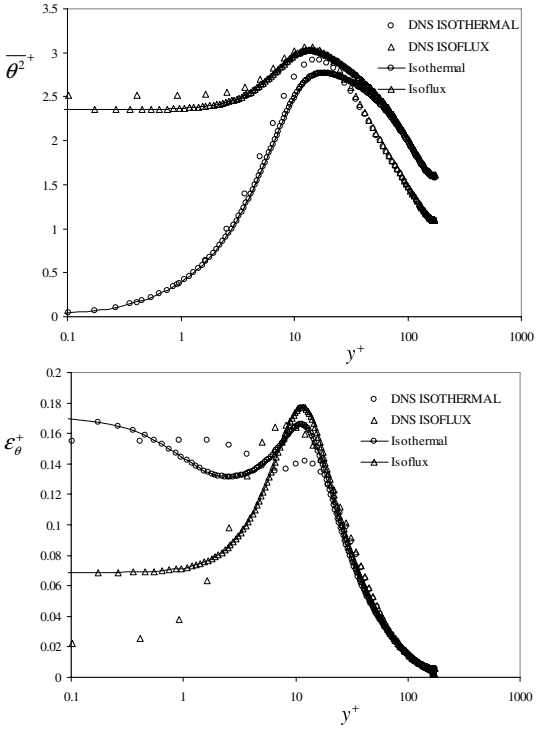

Figure 8: Near-wall $\overline{\theta^2}$ and ε_θ profiles for the limiting isothermal and isoflux thermal boundary condition cases with the modified thermal field modelling.

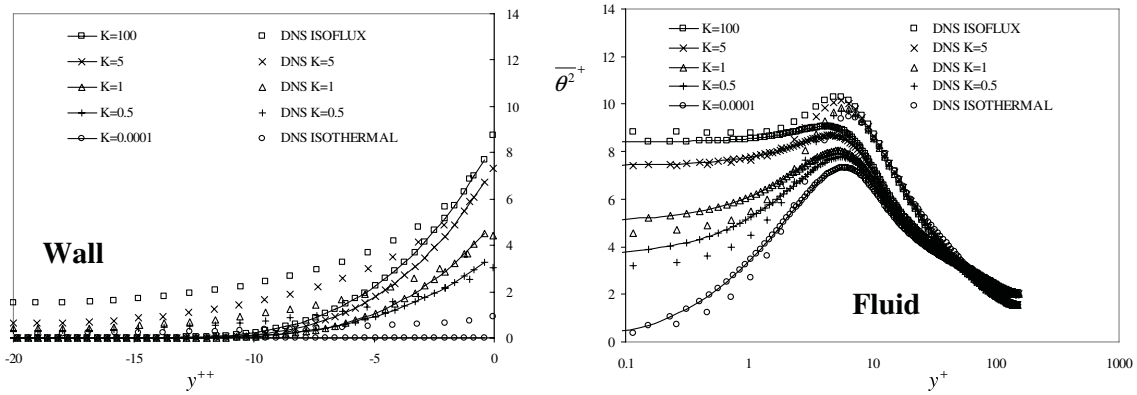

Figure 9: $\overline{\theta^2}$ profiles across the fluid and solid regions for different thermal activity ratios using the modified dynamic and thermal field models.

appear are traditionally split as follows:

$$2\alpha^2 \overline{\frac{\partial\theta}{\partial x_l}\left[\frac{\partial}{\partial x_l}\left(\frac{\partial}{\partial x_j}\left(\frac{\partial\theta}{\partial x_j}\right)\right)\right]} = \frac{\partial}{\partial x_j}\left[\alpha\frac{\partial}{\partial x_j}\left[\alpha\overline{\left(\frac{\partial\theta}{\partial x_l}\frac{\partial\theta}{\partial x_l}\right)}\right]\right] - 2\alpha^2\overline{\left(\frac{\partial^2\theta}{\partial x_j\partial x_l}\right)^2} \quad (18)$$

The first term on the right hand side is then treated as molecular diffusion, and the second term interpreted as being modelled by the various sink terms in equation (6). A reduction of the molecular diffusion term may thus be interpreted as simply modifying the split between the two terms on the right hand side of equation (18), or can equally be thought of as introducing an additional near-wall contribution to the modelled sink terms.

The final set of computations reported here have thus been obtained by including an additional source/sink term of the form

$$S_d = -\frac{\partial}{\partial x_j}\left[c_d(c_p\mu/Pr)\left[1-(\varepsilon_\theta-\tilde{\varepsilon}_\theta)/\varepsilon_\theta\right]\frac{\partial\tilde{\varepsilon}_\theta}{\partial x_j}\right] \quad (19)$$

into the modelled $\tilde{\varepsilon}_\theta$ equation, with the coefficient taken as $c_d = 0.7$. This term is principally significant in the near-wall region for the isoflux case where, as indicated above, it effectively counteracts the molecular diffusion term. With this addition, the coefficient c_{n1} in the near-wall source term of equation (17) was reduced to 0.5. As shown in Figure 10, the addition of the above term does lead to improved near-wall ε_θ and $\overline{\theta^2}$ profiles in the isoflux case.

An additional benefit of the above treatment is that the modification of equation (19) also becomes active across the solid wall region. The corresponding conjugate calculation results are shown in Figure 11, demonstrating that not only is the predicted $\overline{\theta^2}$ improved across the fluid region, but by effectively reducing the diffusion of ε_θ across the solid the

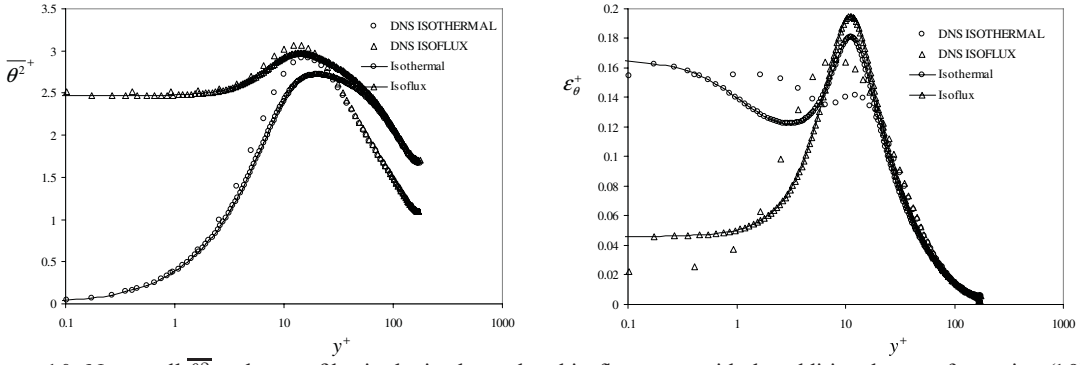

Figure 10: Near-wall $\overline{\theta^2}$ and ε_θ profiles in the isothermal and isoflux cases with the additional term of equation (19).

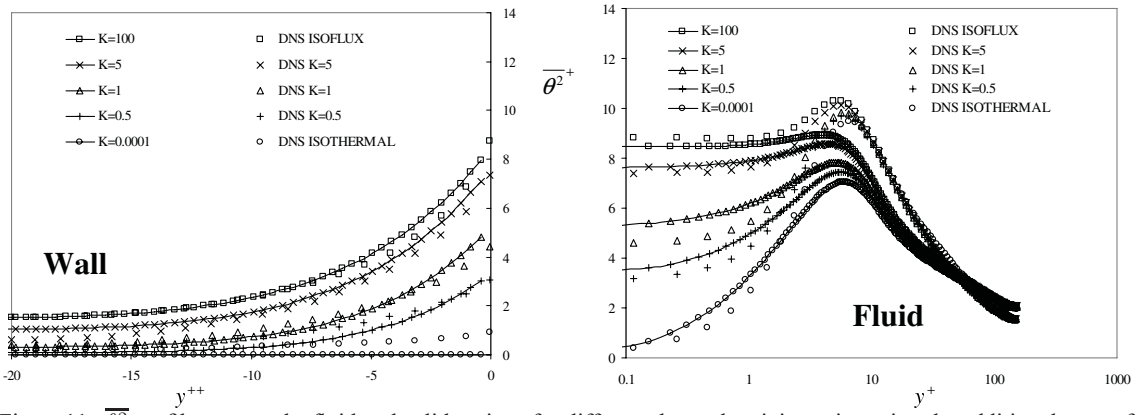

Figure 11: $\overline{\theta^2}$ profiles across the fluid and solid regions for different thermal activity ratios using the additional term of equation (19).

decay of $\overline{\theta^2}$ across this region is also significantly improved, resulting in generally good agreement with the DNS data of Tiselj et al. (2001a).

CONCLUSIONS

The present study has examined the problem of extending the solution of thermal turbulence equations, within a RANS framework, across both fluid and solid wall regions in conjugate heat transfer applications, particularly in order to predict the penetration of temperature fluctuations into the solid. It has been found that, in order to reproduce accurate $\overline{\theta^2}$ profiles across the solid, it is necessary to obtain an accurate representation of the dynamic and thermal field turbulence in the near-wall fluid region.

An existing four-equation model of Hanjalić et al. (1996) has been modified, by including elements based on the three-equation scheme of Suga (1995), specifically aimed at improving the computed near-wall profile of ε. Similar modifications, and a re-interpretation of the split of molecular diffusion/sink terms in the $\tilde{\varepsilon}_\theta$ equation, have been introduced to the thermal turbulence equations to improve the near-wall predictions of $\overline{\theta^2}$ and ε_θ in the two idealised thermal boundary conditions of isothermal and isoflux wall surface. These same modifications have been shown to improve significantly the conjugate heat transfer predictions for a plane channel flow, with the sensitivity of the temperature variance levels to the thermal activity ratio, and the decay of $\overline{\theta^2}$ across the solid wall, reasonably well captured.

Work is currently underway testing the above model in the more complex fluid/solid heat transfer case of a downward-directed, heated, wall jet opposed by a colder upward stream.

REFERENCES

Hanjalić, K., Kenjeres, S., Durst, F. (1996), "Natural convection in partitioned two-dimensional enclosures at higher Rayleigh numbers", *Int. J. Heat Mass Transfer*, **39**, 1407–1427.

Jayatilleke, C. (1969), "The influence of Prandtl number and surface roughness on the resistance of the laminar sublayer to momentum and heat transfer", *Prog. Heat Mass Transfer*, **1**, 193.

Kawamura, H., Ohsaka, K., Abe, H., Yamamoto, K. (1998), "DNS of turbulent heat transfer in channel flow with low to medium-high Prandtl number fluid", *Int. J. Heat Fluid Flow*, **19**, 482–491.

Keshmiri, A. (2006), "Modelling of conjugate heat transfer in near-wall turbulence", MSc Dissertation, School of Mechanical Aerospace & Civil Engineering, The University of Manchester.

Launder, B., Sharma, B. (1974), "Application of the energy-dissipation model of turbulence to the calculation of flow near a spinning disc", *Lett. in Heat Mass Transfer*, **1**, 131–138.

Polyakov, A. (1974), "Wall effect on temperature fluctuations in the viscous sublayer", *High Temperature*, **12**, 286–293.

Suga, K. (1995), "Development and application of a non-linear eddy viscosity model sensitized to stress and strain invariants", Ph.D. thesis, Faculty of Technology, University of Manchester.

Tiselj, I., Bergant, R., Mavko, B., Bajsic, I., Hetsroni, G. (2001a), "DNS of turbulent heat transfer in channel flow with heat conduction in the solid wall", *J. Heat Transfer*, **123**, 849–857.

Tiselj, I., Pogrebnyak, E., Changfeng, L., Mosyak, A., Hestroni, G. (2001b), "Effect of wall boundary condition on scalar transfer in a fully developed turbulent flume flow", *Phys. Fluids*, **13**, 1028–1039.